PERGAMON

Radiation Measurements 35 (2002) 439–455

Radiation Measurements

www.elsevier.com/locate/radmeas

Passive dosimetry aboard the Mir Orbital Station: internal measurements

E.R. Benton[a,*], E.V. Benton[b], A.L. Frank[b]

[a] *Eril Research, Inc., P.O. Box 150788, San Rafael, CA 94915-0788, USA*
[b] *University of San Francisco, 2130 Fulton St., San Francisco, CA 94117-1080, USA*

Received 1 April 2002

The authors dedicate this paper and the companion paper in this issue to the memory of Paul "Tad" Savage, formerly of NASA Ames Research Center, Moffett Field, California, without whose efforts this work would likely not have been possible.

Abstract

Passive radiation dosimeters were exposed aboard the Mir Orbital Station over a substantial portion of the solar cycle in order to measure the change in dose and dose equivalent rates as a function of time. During solar minimum, simultaneous measurements of the radiation environment throughout the habitable volume of the Mir were made using passive dosimeters in order to investigate the effect of localized shielding on dose and dose equivalent. The passive dosimeters consisted of a combination of thermoluminescent detectors to measure absorbed dose and CR-39 PNTDs to measure the linear energy transfer (LET) spectrum from charged particles of $LET_{\infty}H_2O \geqslant 5$ keV/μm. Results from the two detector types were then combined to yield mean total dose rate, mean dose equivalent rate, and average quality factor.

Contrary to expectations, both dose and dose equivalent rates measured during May–October 1991 near solar maximum were higher than similar measurements carried out in 1996–1997 during solar minimum. The elevated dose and dose equivalent rates measured in 1991 were probably due to a combination of intense solar activity, including a large solar particle event on 9 June 1991, and the temporary trapped radiation belt created in the slot region by the solar particle event and ensuing magnetic storm of 24 March 1991.

During solar minimum, mean dose and dose equivalent rates were found to vary by factors of 1.55 and 1.37, respectively, between different locations through the interior of Mir. More heavily shielded locations tended to yield lower total dose and dose equivalent rates, but higher average quality factor than did more lightly shielding locations. However, other factors such as changes in the immediate shielding environment surrounding a given detector location, changes in the orientation of the Mir relative to its velocity vector, and changes in the altitude of the station also contributed to the variation. Proton and neutron-induced target fragment secondaries, not primary galactic cosmic rays, were found to dominate the LET spectrum above 100 keV/μm. This indicates that in low earth orbit, trapped protons in the South Atlantic Anomaly are responsible for the major fraction of the total dose equivalent.

1. Introduction

The Russian Mir Orbital Station can be viewed as the first permanent human outpost in space. Between the launch of the Mir Base Block in February 1986 until its de-orbit in March 2001, over 100 men and women lived and worked aboard Mir for periods of up to 430 days. The on-orbit assembly of the International Space Station (ISS) marks another milestone in the era of a permanent human presence in space. The advent of the ISS will result in both an increase in the number of personnel in low earth orbit (LEO) at any given time and an increase in the duration of each crew member's stay in LEO, leading to an overall increase in the radiation exposure received by humans in space. Accurate prediction of the ionizing radiation dose and dose equivalent of space crews and the subsequent assessment of risk from

* Corresponding author.
E-mail address: eric@erilresearch.com (E.R. Benton).

1350-4487/02/$ - see front matter
PII: S1350-4487(02)00075-6

long-duration radiation exposure has therefore become of greater necessity if the long-term, stochastic effects of space radiation are to be minimized.

Astronauts and experimental payloads aboard LEO spacecraft like the Mir Orbital Station, the NASA Space Shuttle and the ISS are exposed to levels of ionizing radiation far in excess of that encountered on the ground. Charged particles in the form of galactic cosmic rays (GCR), trapped protons and electrons, and particles emitted by the sun during solar flares and coronal mass ejections constantly impinge on the outer surface of the spacecraft. The more energetic of these particles penetrate the skin of the spacecraft and can interact with the mass of the spacecraft and its contents, producing secondary particles in the process. Secondary particles, especially proton- and neutron-induced high LET target fragments, can possess a greater radiobiological effectiveness than the primary particles which produced them.

Dose and dose equivalent prediction and risk assessment are based upon models of the radiation environment in LEO and on models of the transport of ionizing radiation through matter. These models are based in part on in situ measurements of the radiation environment and ongoing monitoring of the LEO radiation environment is needed to validate and update the accuracy of these models. In addition, a more detailed understanding of the different constituent components of the radiation environment in LEO is needed to firmly establish radiation modeling efforts on an analytic and not merely empirical foundation.

The determination of astronaut risk from environmental radiation in LEO requires accurate measurement of dose from the various types of ionizing particles present. Dose equivalent, the radiation quantity currently used for risk assessment, is the product of the dose and an empirically determined radiation quality factor based on the evaluated biological effectiveness of the radiation (ICRP, 1991). The quality factor is a function of linear energy transfer (LET) and, consequently, accuracy in the determination of dose equivalent is dependent on the accuracy of LET spectrum measurements. The accuracy of LET spectrum measurement is particularly important in the LET region above 10 keV/μm where quality factor rises above one. The passive radiation dosimeter developed by our laboratory and used in our measurements of dose and dose equivalent is well-suited to measuring the LET spectrum between 5 and 1500 keV/μm.

Between 1991 and 1998 we conducted a series of passive integrating measurements of the LEO ionizing radiation environment using passive dosimeters located on the interior of the Mir Orbital Station. The measurements were carried out using area passive dosimeters (APDs) developed by our group at the University of San Francisco. Each APD contained two arrays of LiF thermoluminescent detector (TLD) to measure absorbed dose and three mutually orthogonal stacks of CR-39 plastic nuclear track detector (PNTD) to measure the LET spectrum from charged particles of $LET_{\infty}H_2O \geqslant 5$ keV/μm. Results from the CR-39 PNTDs and TLDs were then combined to yield mean total dose rate, mean dose equivalent rate, and average quality factor.

One objective of our ionizing radiation measurements program aboard Mir was the investigation of dose, dose equivalent and mean quality factor as functions of time over a substantial fraction of the eleven year solar cycle. Our first measurements were made between 19 May and 11 October 1991 as part of a Russian-led international collaboration to measure the radiation environment both inside and outside Mir during the Mir-9 mission. This exposure took place during a period of intense solar activity immediately following solar maximum. The solar particle event of 24 March 1991 and the associated disturbances to the interplanetary and geomagnetic fields produced a temporary trapped radiation belt in the slot region between $L = 2$ and 2.5, which was still in the process of decaying during the Mir-9 mission (Shea and Smart, 1996; Gussenhoven et al., 1996). In addition, there were a number of large solar particle events during the Mir-9 mission, itself. Later APD exposures were carried out in conjunction with the NASA/Mir Phase 1 Science Program and began in March 1995 with the NASA-l/Mir-18 mission and lasted until October 1997. Six APDs were exposed inside Mir during the NASA-2/Mir-21 mission between 22 March and 26 September and encompassing solar minimum.

Our radiation measurement program between March 1996 and May 1997 consisted of the simultaneous exposure of up to six APDs distributed throughout the interior of the Mir station. A major objective of the multiple APD exposures was to investigate the effect of the localized shielding distribution within Mir on dose and dose equivalent. Previous measurements made aboard the US Biosatellite-III mission (Benton et al., 1972) and the NASA long duration exposure facility (LDEF) (Benton et al., 1996) demonstrated that short-range secondary particles resulting from the nuclear interaction of protons and neutrons with the constituent nuclei of the spacecraft (including its contents) made a significant contribution to the LET spectrum above 100 keV/μm and could therefore be responsible for a substantial fraction of the total dose and dose equivalent (Benton and Benton, 2001). During readout of the Mir APDs, special emphasis was placed on quantifying the contribution from short-range, high LET particles to the total dose and dose equivalent as a function of APD location and shielding. To carry out this investigation, we developed a method to enhance the short-range particle component when chemically processing the CR-39 nuclear track detectors.

2. Experiment

2.1. Design of the Area Passive Dosimeter

Each APD consisted of a polycarbonate box filled with CR-39 PNTD and arrays of TLD. The APD contained six orthogonal stacks of CR-39 PNTD aligned in three mutually orthogonal directions. In the NASA/Mir Phase

Table 1
Exposures of area passive dosimeters aboard Mir

Mission	Dates	Duration (days)	No. and location
Mir-9	6 June–10 October 1991	126	1 in Base Block
NASA-1/Mir-18	14 March–26 June 1995	129	1 in Base Block
NASA-2/Mir-21	22 March–26 September 1996	188.2	4 in Base Block, 2 in Kvant 2[a]
NASA-3/Mir-22	16 September 1996–22 January 1997	127.2	4 in Base Block, 2 in Kvant 2[a]
NASA-4/Mir-23	12 January–22 May 1997	130.1	4 in Base Block, 2 in Kvant 2[b]

[a]First Kvant-2 APD was exposed during both NASA-2/Mir-21 and NASA-3/Mir-22 missions (305.3 days).
[b]Second Kvant-2 APD was exposed during both NASA-4/Mir-23 and NASA-5/Mir-24 missions (267.5 days).

1B APDs, each CR-39 stack possessed four layers of 4.5 cm × 4.5 cm× ∼ 600 μm thick PNTD separated by layers of 8 μm thick polycarbonate foil. Protective layers of 250 μm thick Lexan polycarbonate covered the top and bottom of each stack. Two TLD arrays, each measuring 1.7 cm×4.2 cm and holding 10 ^{7}LiF TLDs (TLD-700) were placed in the front and back portions of each APD. An assembled Phase 1B APD measured 9.8 cm×9.8 cm×5.5 cm and had a mass of ∼ 0.28 kg. The contents of the Mir-9 and Mir-18 APDs were identical to those exposed during Phase 1B, though the outer dimensions of the earlier APDs were slightly different. During exposure, the APDs were attached to the walls and ceiling of the Mir station by means of Velcro.

2.2. Exposure chronology

Our first measurement aboard Mir took place during the Mir-9 mission in 1991 as part of a collaboration with the Institute of Biomedical Problems (IMBP), Moscow. Our experiment consisted of a single APD exposed within the Base Block (Core module) of Mir for 145 days between 18 May and 11 October, 1991. Our 1991 experiment also included the exposure of passive detectors on the exterior of Mir, the results of which are reported in a companion paper in this issue (Benton et al., 2002).

Our second experiment was conducted during the NASA-1/Mir-18 mission in 1995 as part of the NASA/Mir Phase 1A science program. A single APD was exposed in the Base Block for 129 days, between 14 March and 26 June 1995, during the mission of U.S. astronaut Norm Thaggard.

In 1996–1997 we conducted the Environmental Radiation Measurements on Mir experiment as part of the NASA/Mir Phase 1B science program. Three sets of five to six APDs each were simultaneously exposed throughout the habitable volume of the Mir station during the NASA-2/Mir-21 mission of Shannon Lucid, the NASA-3/Mir-22 mission of John Blaha, and the NASA-4/Mir-23 mission of Jerry Linenger. During each mission in 1996–1997, four APDs were exposed inside the Mir Base Block and two inside the Kvant 2 module. The purpose of the simultaneous APD exposures was to measure cumulative radiation exposure at different locations inside Mir as a function both of time and location. The dates and locations of the APD exposures are listed in Table 1. Locations of the six Phase 1B APDs are listed in Table 2 and illustrated in Figs. 1 and 2. The APDs exposed during the Mir-9 and Mir-18 missions were in roughly the same location as APD-2 shown in Fig. 1.

Table 2
Locations of the APDs inside Mir station during the NASA-2/Mir-21, NASA-3/Mir-22 and NASA-4/Mir-23 missions

Detector	Module	Location
APD-1	Base Block	Door to engineer's cabin
APD-2	Base Block	Ceiling panel #325
APD-3	Base Block	Beneath command console
APD-4	Base Block	Near window #14
APD-5	Kvant 2	Airlock bulkhead
APD-6	Kvant 2	Ceiling panel #303

2.3. APD processing and analysis

Following the return of the APDs to the ground, each APD was disassembled, processed and analyzed at the Physics Research Laboratory at USF. TLD readout was carried out using a standard Harshaw 4000 TLD reader. Ground control TLDs were readout at the same time. Following readout, each TLD was individually calibrated using a NIST certified ^{137}Cs γ-ray source. Doses for each APD were determined by averaging the individual TLD doses from each TLD array.

Two individual layers of CR-39 PNTD from each of three orthogonal stacks in each APD were chemically etched in a solution of 50°C, 6.25 N NaOH for periods of 36 and 168 h, respectively. In order to accurately measure a nuclear track in a layer of CR-39 PNTD, the range of the charged particle that formed the track must be greater than the thickness of bulk detector removed by chemical processing (the bulk etch, B). At the same time, the thickness of bulk detector removed must be large enough to permit the tracks from low LET particles to be sufficiently enlarged to a size where they can be readily located and measured under an optical microscope. Chemical processing in 50°C, 6.25 N NaOH for

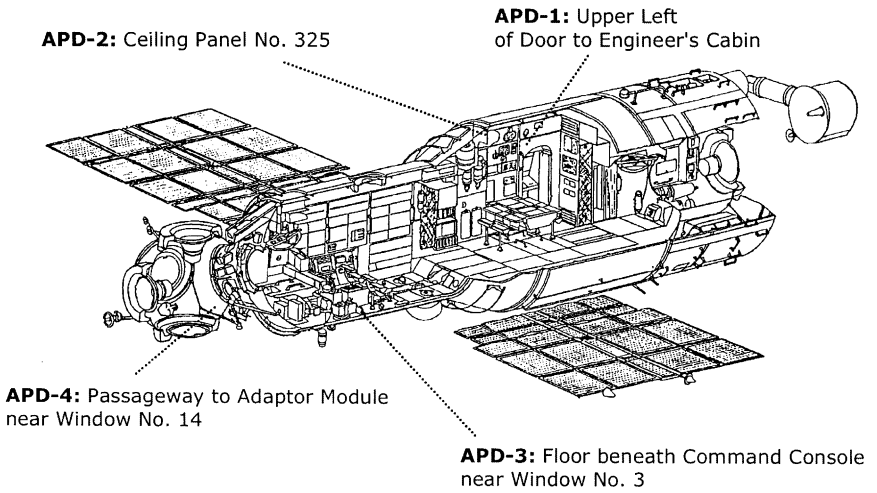

Fig. 1. Locations of APDs in the Mir Base Block during the NASA/Mir Phase 1B exposures. APDs exposed during Mir-9 and NASA-1/Mir-18 were both located near the APD-2 location indicated above.

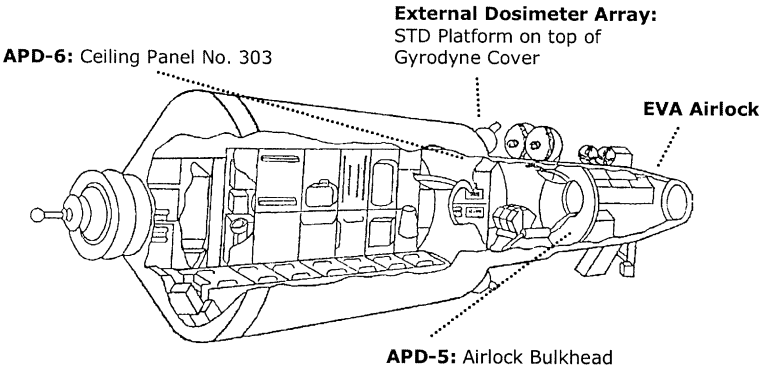

Fig. 2. Locations of APDs in the Kvant 2 module during the NASA/Mir Phase IB exposures.

168 h yields a bulk etch of $\sim$ 40 μm and results in the tracks from low LET particles down to 5 keV/μm being accurately measurable at 250× magnification. However, the high LET secondaries produced in proton and neutron interactions with the nuclei of the detector itself often possess ranges less than 40 μm. Thus, a measurement of the LET spectrum in a detector processed with a bulk etch of 40 μm does not include the substantial contribution from short-range secondaries to the LET spectrum above 50 keV/μm.

In order to include the short-range secondary component, we process a second layer of CR-39 PNTD from a given detector stack in 50°C, 6.25 N NaOH for 36 h. This short etch yields a bulk etch of $\sim$ 8 μm and permits the inclusion of a substantial fraction of the high LET, short range tracks in the LET spectrum measurement. However, tracks from particles of LET less than about 50 keV/μm cannot be accurately measured with 100% efficiency because of their small size. Fig. 3 shows the differential LET fluence spectrum measured in APD-3 exposed during the NASA-4/Mir-23 mission in 1997. Particle tracks of LET $\geqslant$ 5 keV/μm are measured in the 40 μm bulk etch detector, but the large number of short range secondaries of LET $>$ 50 keV/μm are not included. Conversely, the 8 μm bulk etch detector includes tracks with LET in excess of 1000 keV/μm, but tracks of LET $\leqslant$ 50 keV/μm are too small to accurately detect and measure with 100% efficiency. The 8 μm bulk etch detector includes only a fraction of the total fluence of short-range secondaries; some secondaries possess ranges less than the $\sim$ 8 μm bulk etch. However, etching for even shorter periods results in tracks that are too small to accurately resolve using an optical microscope and we are forced to accept this limitation.

PNTDs were read out using a customized version of the ELBEK Automated Track Detector Analysis System (Rusch et al., 1991). The peak in the differential LET spectrum from relativistic Fe at 134.7 keV/μm in H_2O was used as

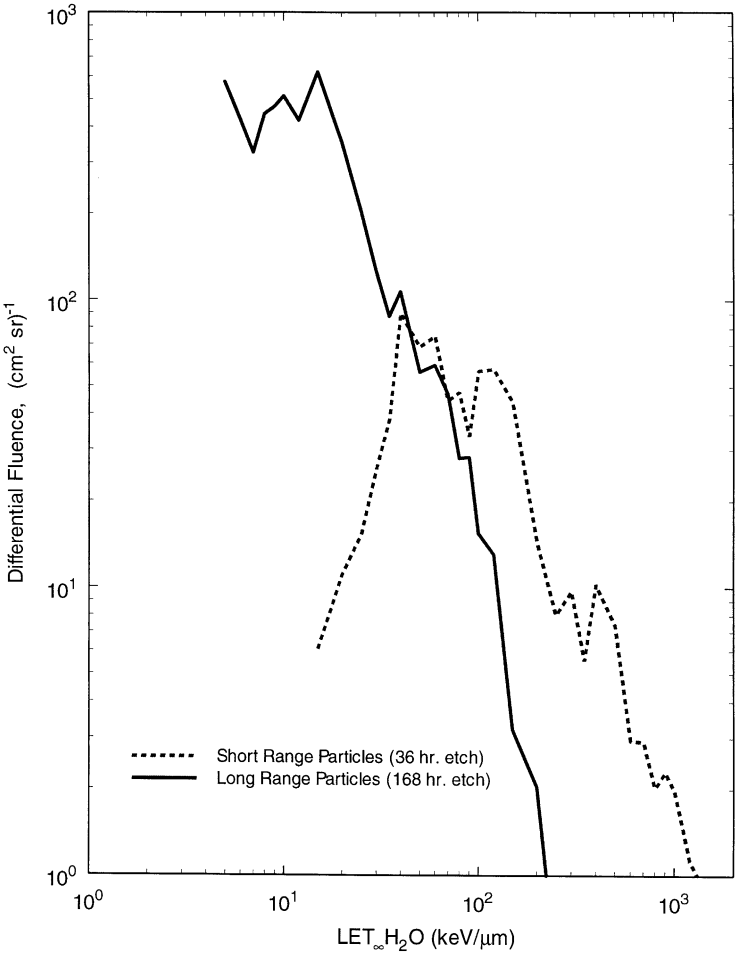

Fig. 3. Differential LET fluence spectrum measured in APD-3 during the NASA-4/Mir-22 mission from the long range (>40 μm) GCR component and short range (>8 μm) secondary + GCR components.

an internal calibration. Track data was converted to LET spectra by means of an empirically derived response function relating LET to the measured reduced etch rate ratio, V_R, for each track. The 40 μm etch and 8 μm etch LET data were folded into a single LET spectrum for each detector orientation. The combined spectra from each of the three orthogonal detector stacks were then averaged into one mean LET spectrum. For the Mir-9 APD, only the 168 h etch was carried out since the 36 h etching technique for short-range secondaries had not yet been developed at the time of this mission.

The TLD and PNTD measurements were combined to yield the total dose and dose equivalent rates for each APD. In this method, the low LET (<10 keV/μm) and high LET ($\geqslant 10$ keV/μm) portions of the dose were separated. An empirical function characterizing the reduced high LET response of LiF TLD was used to correct dose from particles of LET $\geqslant 10$ keV/μm (Benton et al., 2000). The average efficiency is given by

$$\bar{\varepsilon} = \frac{\sum_{10\ \mathrm{keV/\mu m}}^{\mathrm{LET_{max}}} \varepsilon(\mathrm{LET})\mathrm{D}(\mathrm{LET})}{D_{\mathrm{PNTD}\geqslant 10\ \mathrm{keV/\mu m}}}.$$

The low LET component of dose is

$$D_{\mathrm{Low}} = D_{\mathrm{TLD}} - \bar{\varepsilon} D_{\mathrm{PNTD}\geqslant 10\ \mathrm{keV/\mu m}}.$$

The total dose is

$$D_{\mathrm{Total}} = D_{\mathrm{Low}} + D_{\mathrm{PNTD}\geqslant 10\ \mathrm{keV/\mu m}}.$$

The total dose equivalent is given by

$$H_{\mathrm{Total}} = D_{\mathrm{Low}} + H_{\mathrm{PNTD}\geqslant 10\ \mathrm{keV/\mu m}}.$$

Both $D_{\mathrm{PNTD}\geqslant 10\ \mathrm{keV/\mu m}}$ and $H_{\mathrm{PNTD}\geqslant 10\ \mathrm{keV/\mu m}}$ are determined directly from the LET spectrum measured in the CR-39 PNTDs. The average quality factor, $\overline{\mathrm{QF}}$, of the total

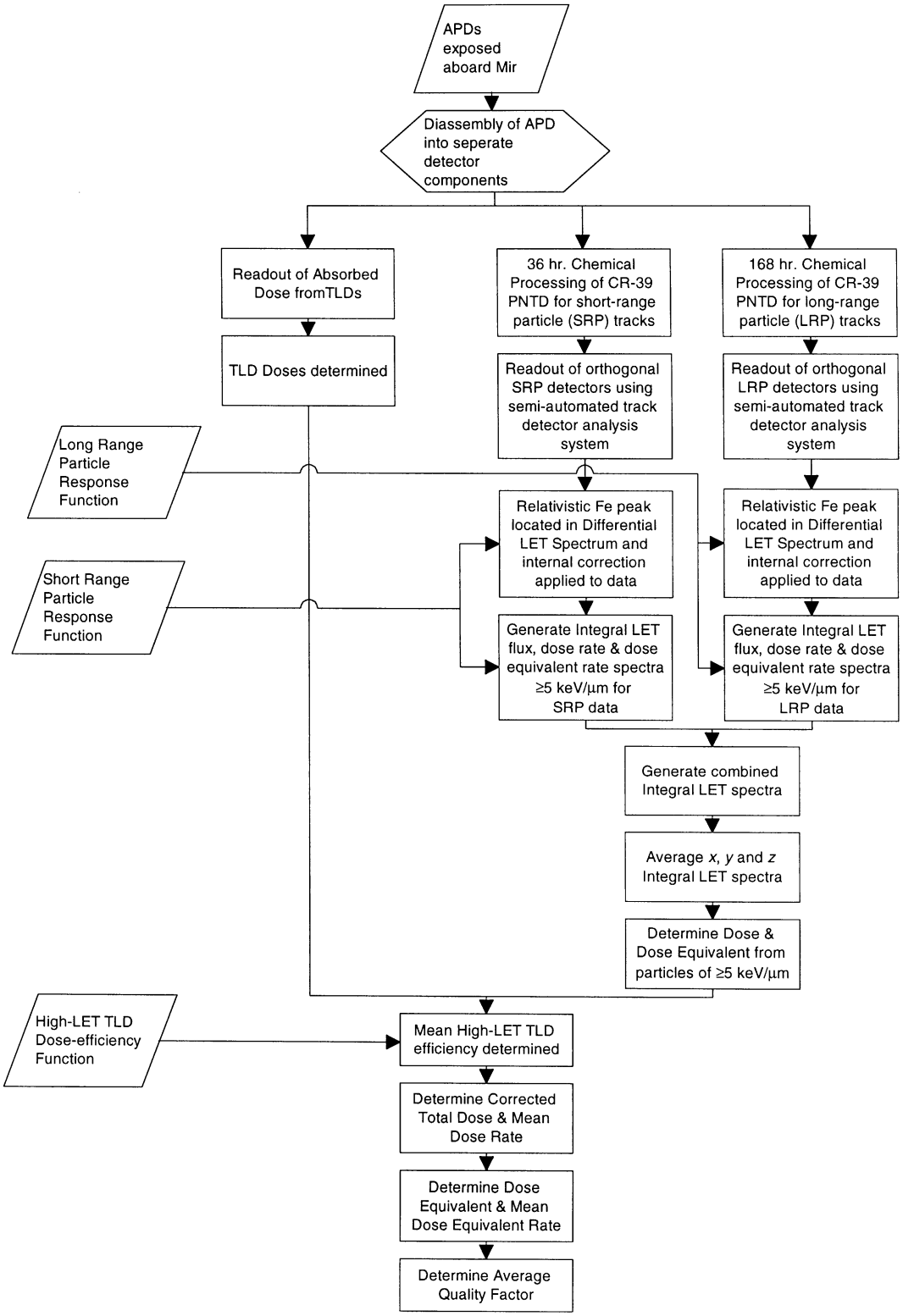

Fig. 4. Flow chart showing procedure used in processing, readout and analysis of passive detectors exposed on Mir. Note that the 1991 Mir-9 detectors were not processed to enhance the short range secondary component.

measured radiation is then:

$$\overline{\mathrm{QF}} = \frac{H_{\mathrm{Total}}}{D_{\mathrm{Total}}}.$$

Mean dose rate and mean dose equivalent rate were found by dividing dose and dose equivalent, respectively, by the total duration of the exposure. The ICRP-60 (ICRP, 1991) definition of quality factor was used in determining dose equivalent. The procedure for post-flight analysis of each APD is shown in the flowchart contained in Fig. 4.

3. Results and discussion

3.1. LET spectra measurements

Integral LET flux, dose rate, and dose equivalent (ICRP-60) rate spectra have been generated from measurements of the APD CR-39 PNTDs. Fig. 5 shows the integral LET flux, dose rate and dose equivalent rate spectra measured in the APD-2 base block location during the Mir-9, NASA-l/Mir-18, NASA-2/Mir-21, NASA-3/Mir-22, and NASA-4/Mir-23 missions. Fig. 6 shows the integral LET flux, dose rate, and dose equivalent rate spectra measured on the NASA-2/Mir-21 mission. Fig. 7 shows the integral LET flux, dose rate, and dose equivalent rate spectra measured from the NASA-3/Mir-22 APDs. Fig. 8 shows the integral LET flux, dose rate and dose equivalent rate spectra measured during the NASA-4/Mir-23 mission.

Fig. 5 shows the integral LET flux, dose rate and dose equivalent rate spectra measured on or near ceiling panel No. 325 in the Base Block of the Mir orbital station during the Mir-9 mission in 1991, the NASA-l/Mir-18 mission in 1995 and the three NASA/Mir Phase 1B missions in 1996–1997. As mentioned above, the LET spectrum measured in the Mir-9 detectors does not include the contribution from short-range secondaries. With the exception of the spectrum measured during Mir-9, there is fairly close agreement amongst the integral LET spectra below 200 keV/μm. The curve measured during the NASA-4/Mir-23 mission lies above the others at LET greater than 200 keV/μm. This may be the result of an increase in station altitude during the NASA-4/Mir-23 mission, changes in the shielding environment immediately surrounding the APD-2 location as equipment was moved around throughout the station, or a change in the orientation of the Mir relative to its velocity vector. The effect of the increased contribution to the integral spectrum above 200 keV/μm measured during the NASA- 4/Mir-23 mission can be more readily seen in the dose rate and dose equivalent rate spectra. Due to the dependence of dose and dose equivalent on LET, small increases in the flux at high LET lead to substantial increases in dose and dose equivalent when compared to the spectra measured during the other NASA/Mir missions.

For LET > 60 keV/μm, the Mir-9 spectrum falls off more rapidly with increasing LET than the other spectra, as expected from the lack of the short-range secondary component in the Mir-9 measurement. However, for LET less than 60 keV/μm, the Mir-9 spectrum lies significantly above that measured during the other four Mir missions. The Mir-9 mission took place in 1991 following solar maximum while the other four missions occurred during the 1995–1997 time period encompassing solar minimum. The possible causes for this difference are discussed in greater detail below.

In Fig. 6, the integral LET flux spectra measured for the five APDs included in the NASA-2/Mir-21 missions show close agreement throughout the entire measured range from 5 to 1500 keV/μm. The curve from APD-6 lies somewhat below the others for LET $\geqslant 100$ keV/μm. The high LET region ($\geqslant 100$ keV/μm) is primarily made up of short-range (~ 8 μm) secondary particles produced in target fragmentation events when neutrons and primary protons interact with the C and O nuclei of the detector. Greater shielding at the APD-6 location is seen as both a decrease in total dose and an increase in the relative number of target fragment events. Most of the spectra are seen to change slope between 250 and 350 keV/μm. This knee occurs at the approximate maximum LET for α-particles ($\sim$ 230 keV/μm). Below this knee, most of the LET spectra is believed to be made up of knockout protons and α-particles produced in target fragmentation events, from proton recoils produced in interactions with secondary neutrons, and low energy primary protons. High energy GCRs of $Z \geqslant 5$ make a smaller contribution. The spectrum above $\sim$ 300 keV/μm is the result of GCR and the heavier target fragments. The lower rate of production of these heavier fragments relative to protons and α-particles is most likely the cause of the steepening slope above $\sim$ 300 keV/μm. Mean dose and dose equivalent rate spectra for the NASA-2/Mir-21 APDs, generated from the averaged flux results, are also shown in Fig. 5. In keeping with the LET flux spectra measurements, there is good agreement between all the dose rate and dose equivalent rate curves.

The integral LET flux measurements made in CR-39 PNTDs exposed during the NASA-3/Mir-22 mission, shown in Fig. 7, are similar to those measured in the NASA-2/Mir-21 mission (Fig. 6). There is fairly close agreement amongst the four spectra measured, except at high LET ($\geqslant 100$ keV/μm). In the high LET region, APD-2 lies below the other curves, while APD-6 in Kvant 2, is the highest. The most likely reason for this difference is a change in the shielding environments surrounding those locations. Another possible explanation is a change in the orientation of the station during the NASA-3/Mir-22 mission. The integral LET dose rate spectra measured in the NASA-3/Mir-22 APDs show a similar trend. Over most of the measured

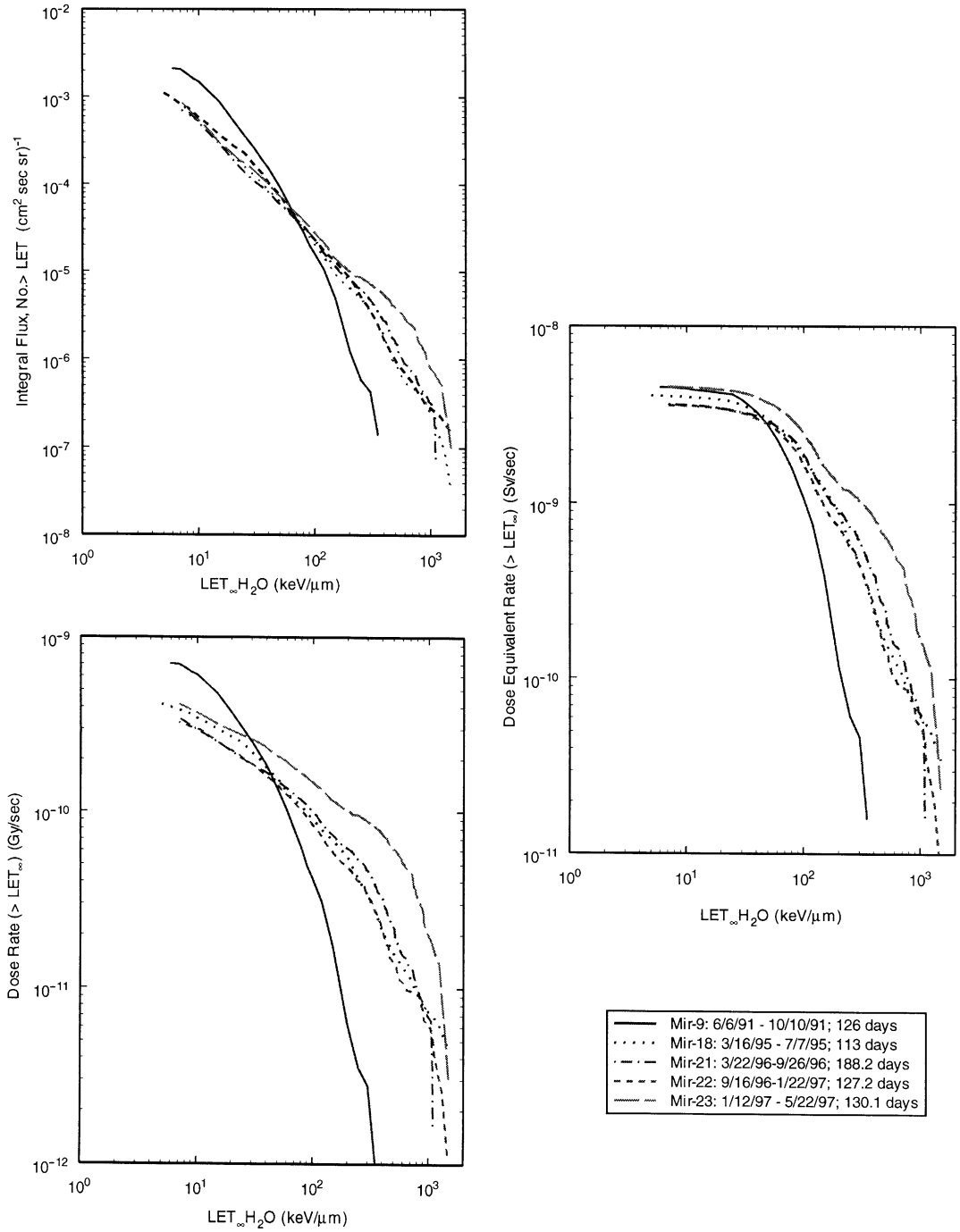

Fig. 5. Mean integral LET flux, dose rate, and dose equivalent rate spectra measured in 1991 and between 1995–1997. The 1991 spectra do not include the contribution from short range, high LET secondaries.

range, APD-6 in the Kvant 2 module has the highest dose rate while APD-2, on ceiling panel No. 325 in the Base Block is the lowest. The APD-6 location was probably the most heavily shielded location and thereby received the greatest flux of high LET, short range secondaries.

As with the NASA-2/Mir-21 and NASA-3/Mir-22 LET flux spectra, the integral LET flux spectra measured on the

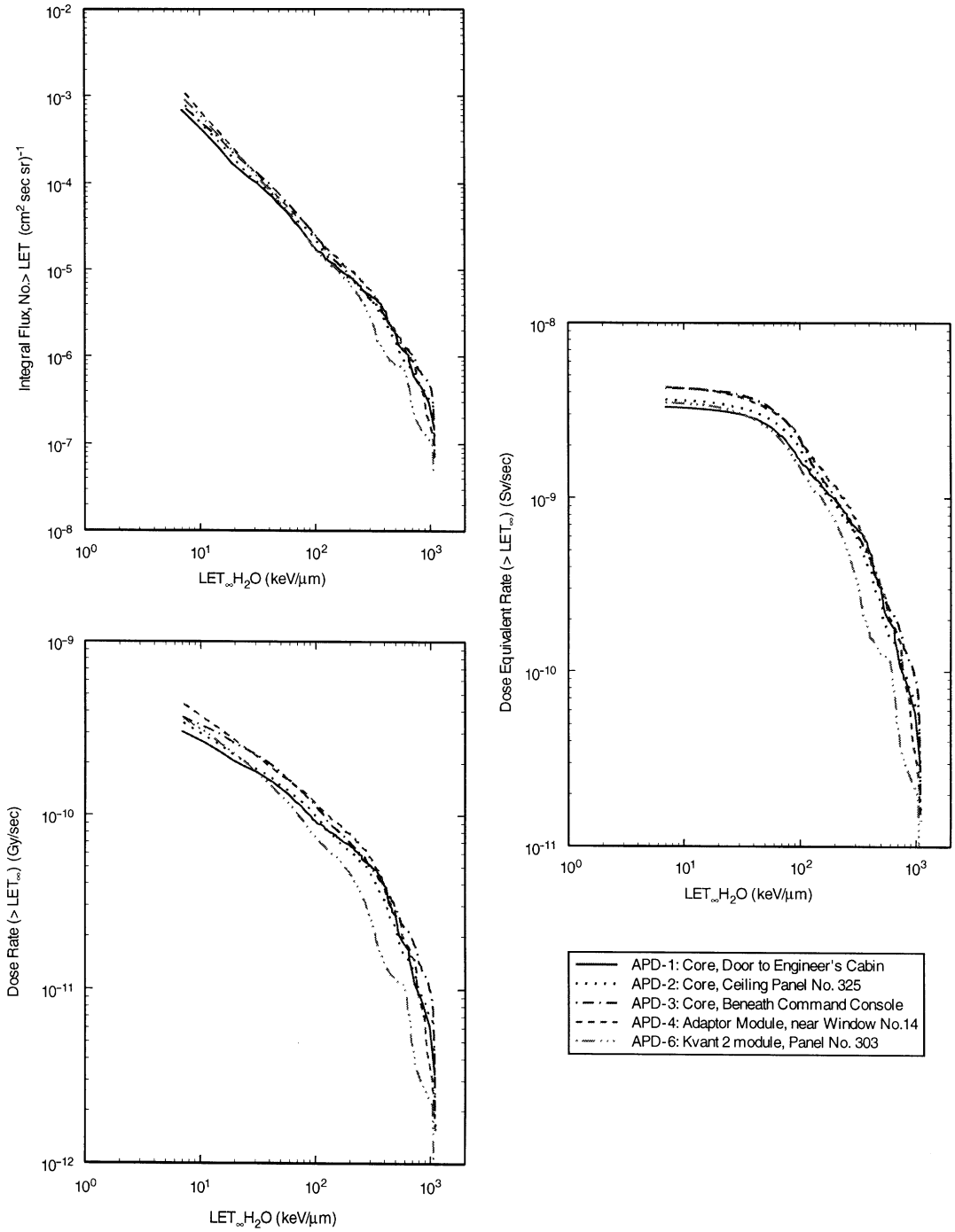

Fig. 6. Mean integral LET flux, dose rate, and dose equivalent rate spectra measured during the NASA-2/Mir-21 mission (3/22/96–9/26/96, 188.2 days).

NASA-4/Mir-23 mission, shown in Fig. 8, are in fairly close agreement throughout most of the measured range. Only at LET $\geqslant$ 100 keV/μm is there much variation. Here APD-3, near the Window No. 3 beneath the command console in the Base Block received the lowest high LET contribution, while APD-2 had the highest. This result is further reflected

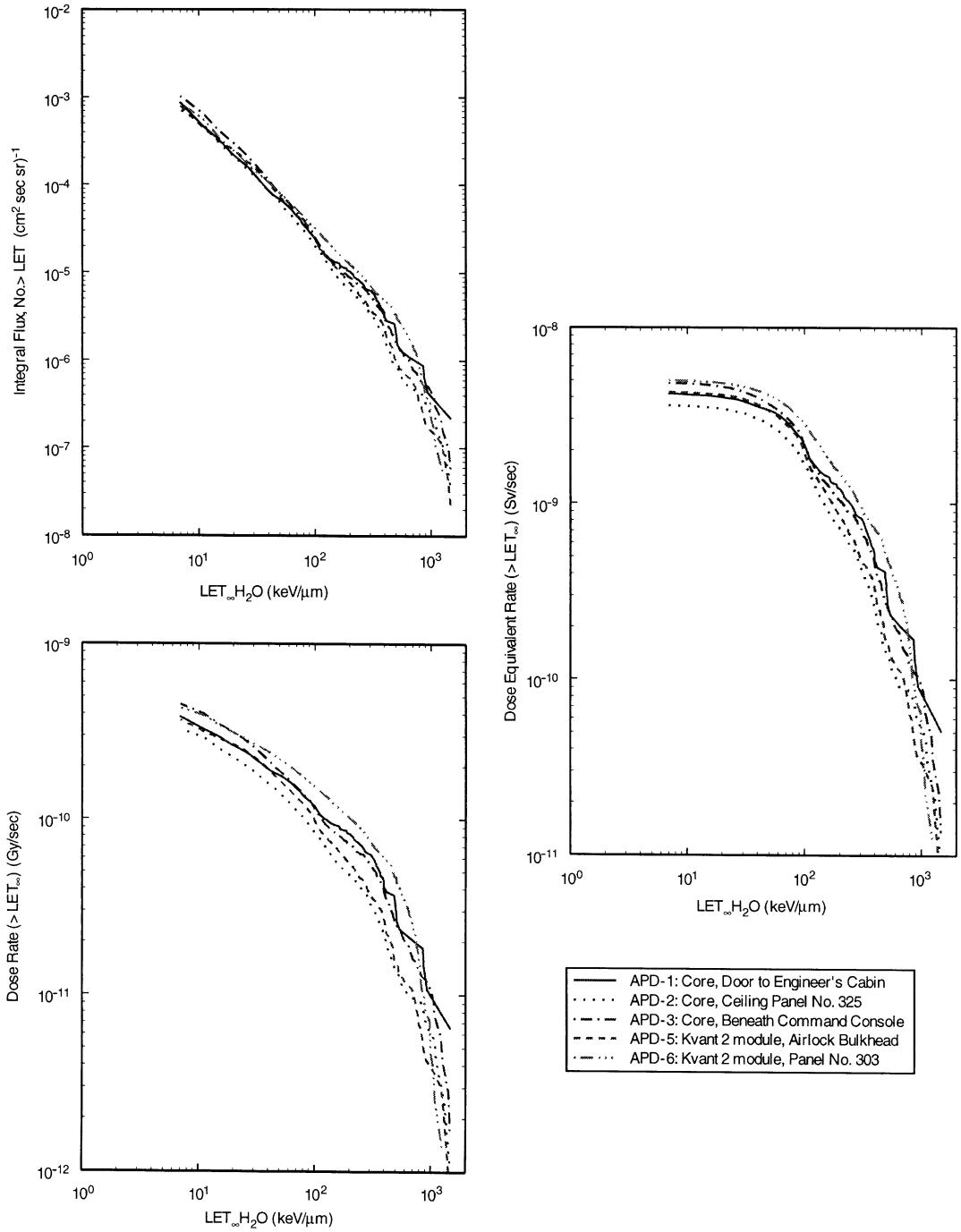

Fig. 7. Mean integral LET flux, dose rate, and dose equivalent rate spectra measured during the NASA-3/Mir-22 mission (9/16/96–1/22/97, 127.2 days).

in the dose and dose equivalent rate spectra. As with the previous missions, the most likely explanation for this difference is a change in the shielding environment immediately surrounding the detectors and/or a change in the orientation of the station.

3.2. Comparison of USF PNTD and JSC-TEPC LET spectra

A comparison of the NASA-2/Mir-21 integral lineal energy transfer flux spectrum measured by the NASA

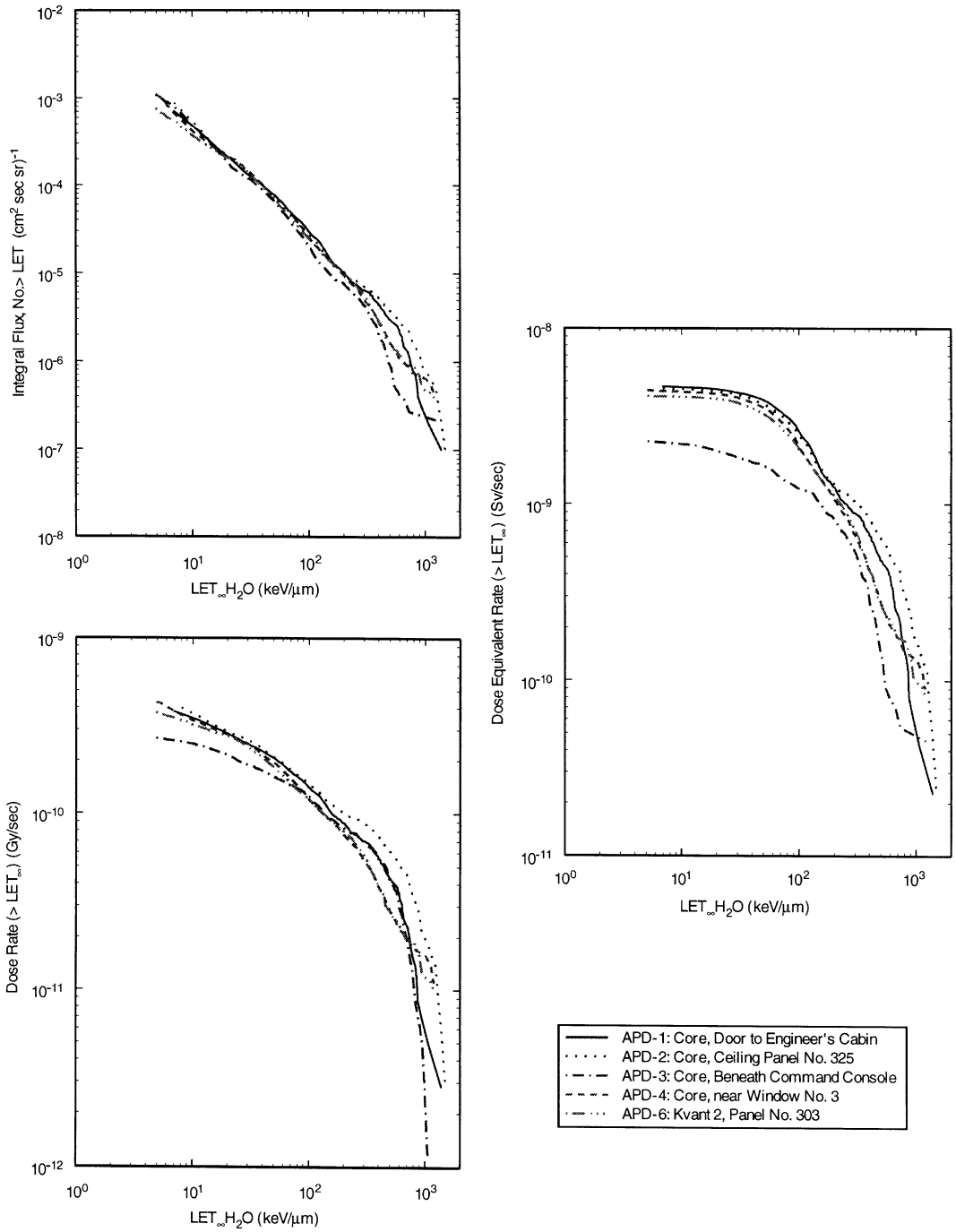

Fig. 8. Mean integral LET flux, dose rate, and dose equivalent rate spectra measured during the NASA-4/Mir-23 mission (1/12/97–5/22/97, 130.1 days).

Johnson Space Center Tissue Equivalent Proportional Counter (JSC-TEPC) with the PNTD results is shown in Fig. 9 (Badhwar, 1998). The two spectra for both types of detector are comparable over almost the entire LET range shown. The deviation of the results below about 20 keV/μm is due to a fall off in the detection efficiency of the PNTDs. Differences above about 100 keV/μm are expected due to the differing elemental compositions of the two types of detector

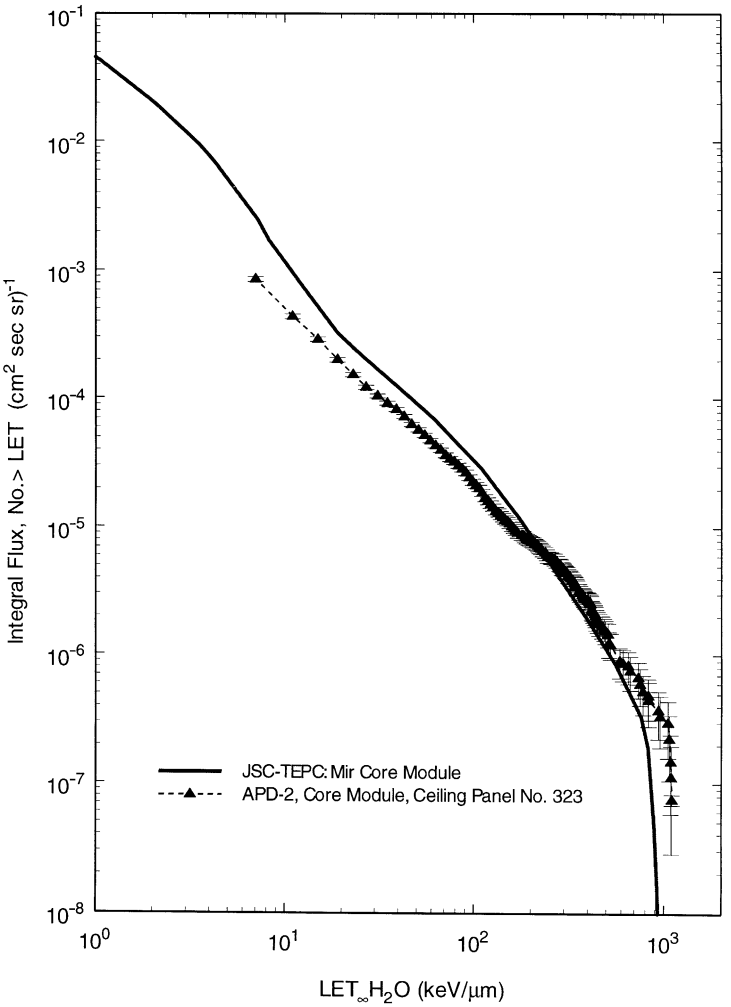

Fig. 9. Integral LET flux spectra measured during the NASA-2/Mir-21 mission by APD-2 and the NASA-JSC TEPC in the Mir Base Block.

media. Above 100 keV/μm, most of the spectrum is produced by neutron and proton-induced, short-range, high LET target fragments. Target fragment production is dependent on the elemental composition of the medium through with the primary protons pass. The greater concentration of C and O nuclei per unit volume in the CR-39 PNTDs versus the sensitive volume of the TEPC leads to the higher PNTD spectrum in the LET region above 100 keV/μm.

3.3. Dose and dose equivalent rate measurements

Table 3 lists the total mean dose and dose equivalent rates, and average quality factors measured at or near Ceiling Panel No. 325, the APD-2 location in the Base Block during the Mir-9 and NASA-l/Mir-18 missions as well as during the NASA/Mir Phase 1B missions in 1996–1997. The mean total dose rate measured during the Mir-9 mission in 1991, near solar maximum, was 365 μGy/d. This was significantly higher than the 273–296 μGy/d dose rate measured during those missions encompassing solar minimum and, at first sight, is contrary to expectations. Similarly, the dose equivalent rate measured during the Mir-9 mission, 653 μSv/d, was larger than the 564–644 μSv/d dose equivalent rate measurements made during solar minimum. Dose and dose equivalent rates from both GCR and LEO trapped protons are expected to be lower during solar maximum than during solar minimum. The cause of the elevated dose and dose equivalent rate measurements from the 1991 Mir-9 APD is not fully understood. Because both the total and high LET dose rates are consistently larger for Mir-9 than for the other missions, it appears unlikely that the Mir-9 detectors could have been contaminated by exposure to some unknown radiation source either during handling and transport on the ground prior to or following the

Table 3
Measured dose rates and dose equivalent rates at or near ceiling panel No. 325 in the Base Block of the Mir Orbital Station during five Mir missions. High LET values are for LET $\geqslant$ 10 keV/μm

Mission	Time	Dose rate (μGy/d)	High LET dose rate (μGy/d)	High LET contribution to dose (%)	Dose equivalent rate (μSv/d)	High LET dose equivalent rate (μSv/d)	High LET contribution to dose equivalent (%)	Mean quality factor
Mir-9	18 May–11 October 1991	365 ± 46	46.0 ± 1.2	12.6	653 ± 42	334 ± 13	51	1.79 ± 0.25
Mir-18	14 March–26 June 1995	273 ± 40	29.9 ± 3.1	10.9	589 ± 101	346 ± 47	59	2.16 ± 0.49
Mir-21	22 March–26 September 1996	296 ± 15	24.6 ± 0.8	8.3	581 ± 18	309 ± 11	53	1.96 ± 0.12
Mir-22	16 September 1996–22 January 1997	281 ± 12	25.3 ± 0.6	9.0	564 ± 15	308 ± 8	55	2.00 ± 0.10
Mir-23	12 January–22 May 1997	285 ± 14	30.9 ± 1.3	10.8	644 ± 21	390 ± 16	61	2.26 ± 0.14

Table 4
Measured dose rates and dose equivalent rates on the NASA-2/Mir-21 mission (3/22/96–9/26/96, 188.2 days) using TLDs and CR-39 PNTDs, and contributions to total dose rates and dose equivalent rates from particles, including target fragments, of LET $\geqslant$ 10 keV/μm

Detector No.	Location	Dose rate (μGy/d)	High LET dose rate (μGy/d)	High LET contribution to dose (%)	Dose equivalent rate (μSv/d)	High LET dose equivalent rate (μSv/d)	High LET contribution to dose equivalent (%)	Mean quality factor
APD-1	Core, door to engineer's cabin	336 ± 19	22.6 ± 1.1	6.7	595 ± 25	282 ± 15	47	1.77 ± 0.14
APD-2	Core, ceiling panel #325	296 ± 15	24.6 ± 0.8	8.3	581 ± 18	309 ± 11	53	1.96 ± 0.12
APD-3	Core, beneath command console	417 ± 21	27.8 ± 0.7	6.7	752 ± 22	363 ± 9	48	1.80 ± 0.10
APD-4	Adaptor, near window #14	290 ± 15	30.8 ± 0.9	10.6	622 ± 19	363 ± 12	58	2.14 ± 0.13
APD-6	Kvant 2, ceiling panel #303	279 ± 8.4	26.1 ± 0.7	9.3	551 ± 17	297 ± 8	54	1.97 ± 0.12

mission, or during the mission itself. The total dose rate is dominated by low LET radiation ($<$ 10 keV/μm) measured by TLDs, while the high LET dose rate ($\geqslant$ 10 keV/μm) was measured by the CR-39 PNTDs. It bears repeating that the Mir-9 measurements do not include the contribution from short-range, high LET secondary particles. Had it been possible to include this component, the difference between the Mir-9 measurements and those made near solar minimum would have been even greater. The most likely cause of the elevated dose and dose equivalent rates measured during Mir-9 is the additional trapped particle flux accrued during passage of the Mir through the temporary belt created in the slot region by the 24 March 1991 solar particle event and subsequent magnetic storm. In addition, the period during which the Mir-9 measurements were made was one of intense solar activity with numerous solar particle events, including a relatively large event on 9 June 1991. These large events were observed aboard Mir by the R-16 operational dosimeter (Mitrikas and Tsetlin, 1995) and the Liulin portable particle spectrometer (Dachev et al., 1999).

Table 4 summarizes the total mean dose rate, mean dose equivalent rate, and the mean quality factor determined from combined TLD and CR-39 PNTD results from the NASA-2/Mir-21 APDs. Also shown in Table 4 are the doses and dose equivalents from particles of LET $\geqslant$ 10 keV/μm and their relative contributions to total dose and dose equivalent rates. Tables 5 and 6 summarize similar results for the NASA-3/Mir-22 and the NASA-4/Mir-23 APDs, respectively.

During the NASA-2/Mir-21 mission, total dose rate varied from 279 μGy/d for APD-6 in the heavily shielded Kvant 2 location to 417 μGy/d for APD-3 in the lightly shielding Base Block location underneath the command console. Dose equivalent rates on this mission ranged from 551 to 752 μSv/d, again at the APD-6 and APD-3 locations respectively. The contribution from particles of LET $\geqslant$ 10 keV/μm to total dose rate varied from 6.7% for the APD-1 and APD-3 locations to 10.6% for the APD-4 location and was 9.3% for APD-6. This reflects the larger flux of low LET particles at the lightly shielded APD-3 location as compared to the larger number of neutron and proton-induced secondaries in the more heavily shielded APD-4 and APD-6 locations. This effect is even more noticeable when looking at the contribution of particles of

Table 5
Measured dose rates and dose equivalent rates on the NASA-3/Mir-22 mission (9/16/96–1/22/97, 127.2 days) using TLDs and CR-39 PNTDs, and contributions to total dose rates and dose equivalent rates from particles, including target fragments, of LET $\geqslant$ 10 keV/μm

Detector No.	Location	Dose rate (μGy/d)	High LET dose rate (μGy/d)	High LET contribution to dose(%)	Dose equivalent rate (μSv/d)	High LET dose equivalent rate (μSv/d)	High LET contribution to dose equivalent (%)	Mean quality factor
APD-1	Core, door to engineer's cabin	319 ± 17	28.3 ± 1.5	8.9	649 ± 28	358 ± 22	55	2.03 ± 0.17
APD-2	Core, ceiling panel #325	281 ± 12	25.3 ± 0.6	9.0	564 ± 15	308 ± 8	55	2.00 ± 0.10
APD-3	Core, beneath command console	390 ± 17	34.5 ± 0.8	8.8	768 ± 21	412 ± 11	54	1.97 ± 0.10
APD-5[a]	Kvant 2, airlock bulkhead	431 ± 19	27.3 ± 0.6	6.3	770 ± 21	366 ± 9	48	1.79 ± 0.09
APD-6	Kvant 2, ceiling panel #303	278 ± 12	33.7 ± 0.9	12.1	674 ± 17	429 ± 12	64	2.42 ± 0.12

[a] APD-5 was exposed for both the NASA-2 and NASA-3 missions for a total of 305.3 days.

LET $\geqslant$ 10 keV/μm to the total dose equivalent. For APD-1, 47% of the dose equivalent was from particles of LET $\geqslant$ 10 keV/μm while for APD-4 it was 58% and for APD-6 it was 54%.

While the higher LET particles make a relatively small contribution to total dose, because of their higher LETs, they contribute a substantial fraction of the total dose equivalent. The lightly shielded APD-1 and APD-3 locations had the lowest mean quality factor—1.77 and 1.80, respectively—while the mean quality factor for the more heavily shielded APD-4 and APD-6 locations was 1.97 and 2.14, respectively. It is important to note that the more heavily shielded location produced the higher mean quality factor.

The observation that the least shielded location yielded both the highest mean dose rate and the lowest mean quality factor while the most heavily shielded location produced the smallest mean dose rate and highest quality factor can again be seen in the results from the NASA-3/Mir-22 mission shown in Table 5. The mean dose rate at the APD-6 location was 278 μGy/d, but the mean dose equivalent rate was 674 μSv/d and the mean quality factor was 2.42. This reflects the fact that a larger proportion of the total flux of particles incident on the APD-6 location was in the form of high LET target fragments from proton- and neutron-induced secondary reactions and from primary GCR. APD-5, exposed at the airlock bulkhead of the Kvant 2 module during both the NASA-2/Mir-21 and NASA-3/Mir-22 missions measured the highest mean dose rate, 431 μGy/d, and the highest mean dose equivalent rate, 770 μSv/d, but had the lowest mean quality factor, 1.79. Like the other lightly shielded locations, the airlock bulkhead received a larger flux of low LET particles, principally primary high energy protons in the South Atlantic Anomaly, than did the more heavily shielded locations.

During the NASA-4/Mir-23 mission, mean dose and dose equivalent rates, shown in Table 6, tended to be slightly higher than during the previous two missions, with the exception of APD-3. This increase may in part have been due to a small increase in altitude of the station. On 15 April 1997 the Mir was boosted from a mean altitude of 385 km to 390 km. While this altitude increase is small, the flux of primary protons in the South Atlantic Anomaly is highly altitude dependent and even small increases in altitude can lead to noticeable increases in the proton dose. The other cause of the increase in dose rate may be a change in the orientation of the station. The proton environment in LEO is directionally dependent with the leading edge of the station receiving a higher proton flux than the station's trailing edge. As on the two previous missions, the highest dose rate was seen in the least shielded APD-3 location during the NASA-4/Mir-23 mission. Only 5.2% of the dose measured by the APD-3 detector was from particles of LET $\geqslant$ 10 keV/μm. Similarly, the dose equivalent at this location was 537 μSv/d as compared to 661 μSv/d in the more heavily shielded APD-4 location. However, particles of LET $\geqslant$ 10 keV/μm contributed only 35% of the total dose equivalent in APD-3 as compared to 57% in APD-4. Mean quality factor was 1.47 for APD-3 and 2.12 for APD-4 during NASA-4/Mir-23.

APD-6 remained on board Mir in its heavily shielding location in the Kvant-2 module until the end of the NASA-5/Mir-24 mission so that it could be compared with the External Dosimeter Array that was deployed during these two missions. Total mean dose rate was 295 μGy/d, mean dose equivalent rate was 622 μSv/d, and mean quality factor was 2.11.

During the NASA/Mir Phase 1B program, mean dose rate varied by as much as a factor of 1.55 between different locations during a given mission. Mean dose equivalent

Table 6
Measured dose rates and dose equivalent rates on the NASA-4/Mir-23 mission (1/12/97–5/22/97, 130.1 days) using TLDs and CR-39 PNTDs, and contributions to total dose rates and dose equivalent rates from particles, including target fragments, of LET $\geqslant$ 10 keV/μm

Detector No.	Location	Dose rate (μGy/d)	High LET dose rate (μGy/d)	High LET contribution to dose (%)	Dose equivalent rate (μSv/d)	High LET dose equivalent rate (μSv/d)	High LET contribution to dose equivalent (%)	Mean quality factor
APD-1	Core, door to engineer's cabin	335 ± 16	29.5 ± 1.1	8.8	706 ± 23	400 ± 16	57	2.11 ± 0.13
APD-2	Core, ceiling panel #325	285 ± 14	30.9 ± 1.3	10.8	644 ± 21	390 ± 16	61	2.26 ± 0.14
APD-3	Core, beneath command console	367 ± 16	19.2 ± 0.3	5.2	537 ± 16	188 ± 4	35	1.47 ± 0.07
APD-4	Adaptor, near window #14	311 ± 13	27.7 ± 0.3	8.9	661 ± 13	377 ± 4	57	2.12 ± 0.09
APD-6[a]	Kvant 2, ceiling panel #303	295 ± 13	25.6 ± 0.3	8.7	622 ± 13	352 ± 4	57	2.11 ± 0.09

[a] APD-6 was exposed for both the NASA-4 and NASA-5 missions for a total of 267.5 days.

rates varied by a smaller factor, as much as 1.37 during a given mission. NASA-4/Mir-23, the mission with the smallest variation in dose and dose equivalent rates as a function of exposure location, yielded the largest variation in average quality factor: 1.54. While differences in the relative shielding of different APD locations throughout the Base Block and Kvant 2 modules are undoubtedly responsible for much of the variation in dose and dose equivalent rate, this variation was not consistent over the course of the three NASA/Mir Phase 1B missions. Thus the situation is more complicated and other factors besides the localized shielding environment must have played a role.

Besides the localized shielding environment, change in altitude and station orientation are probably the other two largest factors contributing to the difference in dose and dose equivalent rates measured at the same location inside the Mir over an extended period of time. Dose rate increases by roughly a factor of 2 for every 50 km increase in altitude. Since records of the altitude of the Mir Station as a function of time are, in principal, available, it should be possible to include altitude variation in any attempt to model the dose and dose equivalent rates received inside Mir. Similarly, in principle there exist records of the orientation of the Mir station relative to its velocity vector over the history of the station that would be helpful in interpreting the variations in dose and dose equivalent rates measured at different locations within Mir during a given time interval. However, attempts to obtain this data have been unsuccessful. With similar measurements now already underway aboard the ISS, researchers must make the ISS management aware of the need for altitude and orientation data to aid in the interpretation of results.

3.4. High-LET contribution from target fragment secondaries

An important conclusion that can be drawn from the simultaneous measurements of the radiation environment as a function of location within the Mir is that lower shielding yields higher dose rate while greater shielding yields a higher mean quality factor. In other words, increased shielding serves to "harden" the spectrum. The hardening of the LET spectrum with increasing shielding can be thought of, in simplistic terms, as a "target fragment cascade" process. High energy trapped protons encountered during passage of the spacecraft through the SAA penetrate the mass of the spacecraft. These primary protons undergo target fragmentation interactions with the constituent nuclei making up the mass of the spacecraft and its contents. The secondary particles resulting from these target fragment interactions include short-range charged particles (knock-out protons and α-particles, heavy recoil nuclei, etc.) and longer-range neutrons. Because the secondary neutrons do not undergo energy loss through direct ionization as they penetrate the spacecraft mass, there is a build-up of secondary neutron flux as shielding increases. These secondary neutrons themselves may undergo target fragment interactions with the nuclei of the spacecraft, producing short-range "tertiary" particles. It is these high-LET charged particles that are directly responsible for the increase in the LET spectrum at high LET ($\geqslant$ 100 keV/μm) with increasing shielding depth.

Additional analysis was carried out on the NASA-2/Mir-21 APD-2 PNTDs in order to separate the long range GCR component from the short range target fragmentation component. Each track on the top surface of the

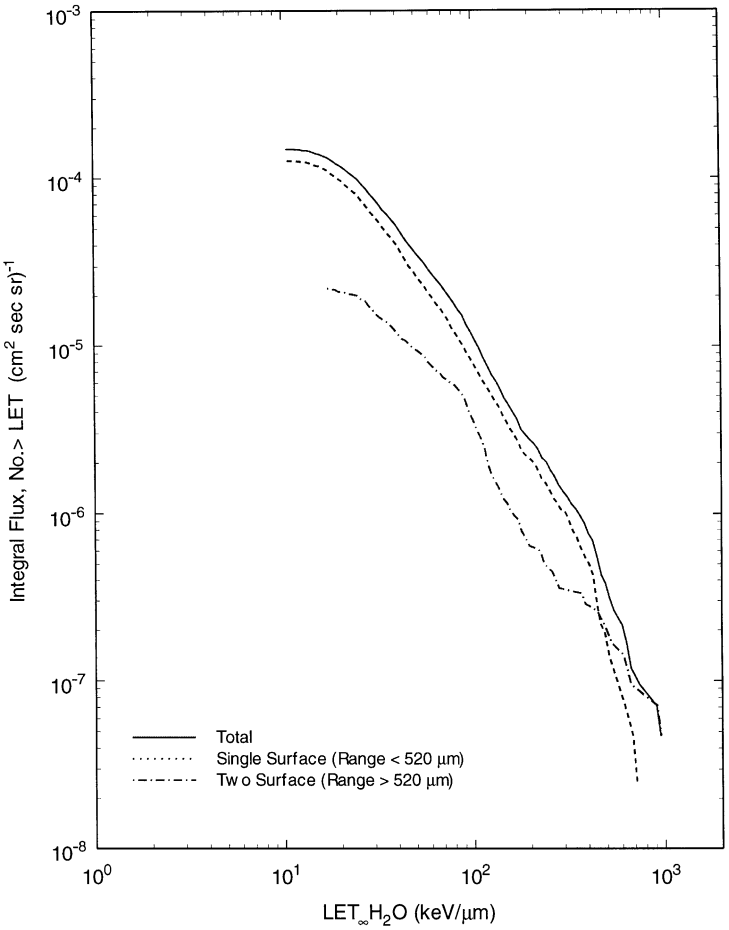

Fig. 10. Integral LET flux spectra of one-surface (target fragments) and two-surface (GCR) tracks measured in NASA-2/Mir-21 APD-2.

detector was projected through the detector and the bottom surface was examined for a companion track produced by the same particle. At LET $\geqslant$ 100 keV/μm, those particles that formed tracks on both top and bottom surfaces of the detector, thus possessing a range in excess of 520 μm, are taken to be primary GCR. Those particles that formed only a single track, thereby possessing a range less than 520 μm, are assumed to be neutron- and proton-induced secondaries. Fig. 10 shows the integral LET flux spectrum measured in the NASA-2/Mir-21 APD-2 from the single surface and two surface particle events, as well as their combined total. Over most of the measured LET range, from 10 to nearly 500 keV/μm, the single surface, target fragmentation events dominate. Only at LET $\geqslant$ 500 keV/μm do the two surface GCR events become the majority. At 100 keV/μm, where the ICRP-60 quality factor is a maximum, the solid majority of events are from target fragmentation.

4. Conclusions

Dosimetric measurements made aboard the Mir Orbital Station in 1991 during solar maximum and in 1996–1997 during solar minimum illustrate the significant contribution made to dose and dose equivalent in LEO from solar particle events. Intensity of both the interplanetary GCR flux and the trapped proton flux in the South Atlantic Anomaly are inversely proportional to the eleven year solar cycle. Dose rate is expected to be a factor of 1.5 to 2 lower during solar maximum than during solar minimum (Badhwar, 2000). However, our mean dose rate measurement in 1991 near solar maximum was 1.23 times greater than our measurement made during the NASA-2/Mir-21 mission during solar minimum. Similarly, our measurement of mean dose equivalent rate made in 1991 was 1.12 times greater than that measured during solar minimum. The differences are actually greater since our 1991 measurements did not include the contribution from short range, high LET target fragments. We

conclude that the increased dose and dose equivalent rates measured near solar maximum were caused by solar activity in the form of the 9 June 1991 solar particle event and the temporary belt formed in the slot region between $L = 2$ and 2.5 by the solar particle event and magnetic storm of 24 March 1991.

Simultaneous measurement of the mean dose rate throughout the habitable volume of the Mir during solar minimum varied by 1.55 as a function of location. Similarly, a factor of 1.37 variation in mean dose equivalent rate as a function of location was measured. Lightly shielded locations tended to yield higher total dose and dose equivalent rates than more heavily shielded locations, but had lower average quality factors. The contribution to total dose and dose equivalent from particles of $LET_{\infty}H_2O \geqslant 10$ keV/μm also tended to be smaller at the lightly shielded locations as compared to those under greater shielding. Thus, while increased shielding served to attenuate a greater fraction of the overall particle flux, it also tended to "harden" the spectrum by increasing the average LET of the flux. This observation is most likely related to the trapped proton flux encountered in then South Atlantic Anomaly. Greater shielding, while attenuating the trapped proton flux, leads to a buildup in secondary neutron flux and, ultimately, an increase in the LET spectrum at high LET via the "target fragment cascade" process.

Additional analysis of the CR-39 PNTDs exposed during solar minimum show that the majority of particles with LET $\geqslant 100$ keV/μm are short range target fragments produced in nuclear interactions between protons and neutrons and the nuclei of the Mir and its contents (target fragmentation), and not primary GCR. Only at LET $\geqslant 500$ keV/μm do primary GCR make a larger contribution to the flux spectrum than do target fragmentation events.

While the immediate shielding environment surrounding a given location plays the major role in explaining the variation in dose and dose equivalent measured throughout the interior of Mir, other factors also influence this variation. Principle among these is the orientation of the Mir relative to its velocity vector. The East/West trapped proton anisotropy present in the South Atlantic Anomaly results in a substantial difference in the proton flux between the leading and trailing edges of the spacecraft. The fact that the Mir was, for the most part, in a fixed orientation relative to its velocity vector (i.e. it was not tumbling) resulted in the leading edge receiving a 2–2.5 times larger flux of trapped protons than the trailing edge (Badhwar, 2000). However, the orientation of Mir was often changed in order to optimize illumination of the solar panels by the sun. This resulted in different parts of the station being the leading edge and greatly complicates any effort to understand and model the radiation exposure of the different APD locations within Mir. Changes in the orbital altitude of Mir—the gradual decay in altitude followed by periodic reboosts—also plays a role in understanding the dose and dose equivalent rates measured at the different APD locations. An important practical lesson learned from conducting dose and dose equivalent rate measurements aboard the Mir Orbital Station and one that is directly applicable to the ISS is the need for altitude and orientation records for the spacecraft as a function of time, in addition to shielding information, to aid in the interpretation of the measured results.

References

Badhwar, G.D., 1998. Private communication.

Badhwar, G.D., 2000. Radiation measurements in low Earth orbit: U.S. and Russian results. Health Phys. 79 (5), 507–514.

Benton, E.R., Benton, E.V., 2001. Space radiation dosimetry in low-Earth orbit and beyond. Nucl. Instrum. Methods B 184, 255–294.

Benton, E.V., Curtis, S.B., Henke, R.P., Tobias, C.A., 1972. Comparison of measured and calculated high-LET nuclear recoil particle exposure on Biosatellite-III. Health Phys. 23, 149–157.

Benton, E.R., Benton, E.V., Frank, A.L., Frigo, L.A., Csige, I., 1996. Secondary particle contribution to the LET spectra on LDEF. Radiat. Meas. 26 (6), 793–798.

Benton, E.R., Frank, A.L., Benton, E.V., 2000. TLD efficiency of ^{7}LiF for doses deposited by high-LET particles. Radiat. Meas. 32 (3), 211–214.

Benton, E.R., Benton, E.V., Frank, A.L., 2002. Passive dosimetry abroad the Mir Orbital Station: external results. Radiat. Meas., this issue, PII: S1350-4487 (02) 00076-8.

Dachev, Ts.P., Tomov, B.T., Matviichuk, Yu.N., Koleva, R.T., Semkova, J.V., Petrov, V.M., Benghin, V.V., Ivanov, Yu.V., Shurshakov, V.A., Lemaire, J.F., 1999. Solar cycle variations of Mir radiation environment as observed by the Liulin dosimeter. Radiat. Meas. 30 (1), 269–274.

Gussenhoven, M.S., Mullen, E.G., Brautigam, D.H., 1996. Improved understanding of the Earth's radiation belts from the CRRES satellite. IEEE Trans. Nucl. Sci. 43 (2), 353–368.

International Commission on Radiological Protection, 1991. 1990 recommendations of the international commission on radiological protection. ICRP Report No. 60, Pergamon Press, Oxford.

Mitrikas, F.G., Tsetlin, V.V., 1995. Mir and other Russian spacecraft orbits examined. Kosm. Issled. 33 (4), 389–394 (in Russian).

Rusch, G., Winkel, E., Noll, A., Heinrich, W., 1991. The Siegen automatic measuring system for track detectors: new developments. Nucl. Tracks Radiat. Meas. 19 (1–4), 261–266.

Shea, M.A., Smart, D.F., 1996. Solar-interplanetary phenomena in March 1991 and related geophysical and technological consequences. Radiat. Meas. 26 (3), 427–432.